MODELING OF SPANDREL ELEMENTS IN URM STRUCTURES WITH RC SLABS OR RING BEAMS

K. Beyer[1] and A. Dazio[2]

Abstract

In many unreinforced masonry (URM) buildings, reinforced concrete (RC) slabs or ring beams maintain the integrity of the building when subjected to seismic loading and redistribute forces between different URM piers. In addition, RC slabs and ring beams contribute to the global stiffness and overturning capacity of the building by acting as horizontal coupling elements between URM piers.

This paper reviews current design approaches concerning the consideration of the contribution of RC slabs and ring beams to the global overturning capacity of buildings with URM piers. Numerical simulations of composite spandrels consisting of RC beam and URM spandrel are performed and the results are compared with experimental evidence from own full-scale tests on composite spandrels. Finally, different wall configurations of URM buildings with RC slabs are analyzed and conclusions concerning the design and analysis of such buildings drawn.

Introduction

Most modern residential buildings in Switzerland or Germany feature unreinforced masonry (URM) walls and flat reinforced concrete (RC) slabs. In other European countries, e.g. Italy, RC ring beams reinforce URM buildings, which do not have RC slabs. RC slabs and ring beams can act as horizontal coupling elements between URM walls, therefore increasing the overturning capacity of URM buildings by transforming the cantilever wall system into a frame system. The degree of coupling introduced by the RC slabs and ring beams depends on

[1] Ecole polytechnique fédérale de Lausanne (EPFL), 1015 Lausanne, Switzerland, katrin.beyer@epfl.ch
[2] EUCENTRE, 27100 Pavia, Italy, alessandro.dazio@eucentre.it

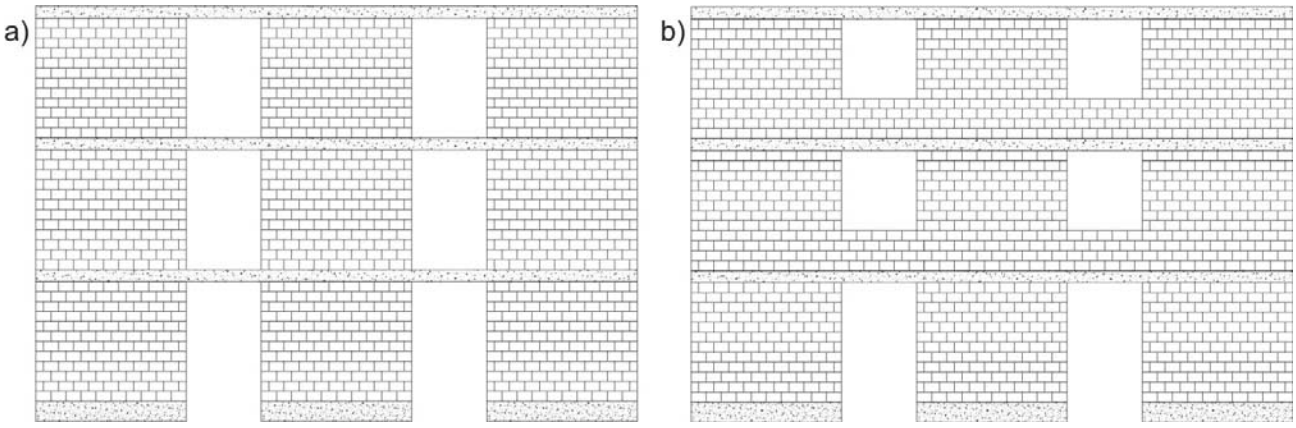

Figure 1. Typical outer wall configurations in modern URM construction with spandrels consisting of the RC slab or ring beam alone (a) and with “composite spandrels”, which feature also a URM spandrel.

Figure 2. Examples of URM buildings corresponding to the wall layouts in Figure 1.

stiffness and strength of these spandrels with respect to those of the walls. In outer walls the spandrel elements can consist of the RC element alone (Figure 1a) or they may include also a masonry spandrel on top of the RC slab or beam (Figure 1b). The former can be found in very modern construction with window units spanning the entire story height (Figure 2a) while the latter configuration is predominant in outer walls of URM buildings with classical window openings (Figure 2b). Since it combines a RC element with a URM spandrel, this type of spandrel is in the following named “composite” spandrel. The RC element can be either part of a RC ring beam or part of a RC slab. For the analysis of the latter an effective slab width is estimated and the slab then treated as a beam. The effective slab width is a function of many parameters; design estimates for the effective slab width for spandrels in URM walls are given, for example, in Priestley *et al.* [Priestley 2007].

Many current design codes neglect the coupling action due to spandrel elements. One main reason for this was the lack of experimental evidence for the behavior of spandrel elements, which also prevented the verification of numerical and mechanical models. For this reason the authors of this paper carried out a large experimental test series on spandrel elements comprising quasi-static tests on five composite spandrels and four masonry spandrels. The objective of this paper is to give a brief overview on the experimental study, to compare the observed mechanism with existing mechanical models for composite spandrels and to present some results of simplified micro-models for a tested composite spandrel as well as an entire wall configuration similar to the one shown in Figure 1b. The paper concludes with an outlook on the planned research work.

Existing design guidelines for composite spandrels

The Italian seismic design code OPCM 3431 [OPCM 2003, 2005] provides guidelines for computing the shear and flexural capacity of spandrel elements in URM buildings. It distinguishes between spandrel elements for which the axial force is either known or unknown. In the first case, the spandrels are treated like piers. In the second, the capacity of the spandrel can only be considered if a strut-and-tie mechanism can develop, i.e. a tension member must be present. In this case the spandrel capacities associated with shear and flexural failure can be estimated as:

- Shear failure $V_s = htf_{vd0}$ **[1]**
- Flexural failure $V_f = F_t \frac{h}{L_{CB}} \left(1 - \frac{F_t}{0.85htf_{hd}}\right)$ **[2]**

where h is the height, t the thickness and L_{CB} the clear span of the spandrel, f_{vd0} the design shear strength in absence of compression, f_{hd} the design compressive strength of the masonry in horizontal direction and F_t the minimum between the tensile strength of the horizontal tensile element and $0.4htf_{hd}$. For a composite spandrel the RC beam can be considered as the tension member, which results therefore for the flexural failure in the strut-and-tie model shown in Figure 3. The strut-and-tie model comprises a compression diagonal in the masonry spandrel, which inclination is determined by the geometry of the spandrel. The RC beam acts as a tension member with a constant axial force along the span of the spandrel.

Priestley *et al.* [Priestley 2007] recommend for practical purposes to neglect the masonry in composite spandrels and to assume that the RC beam only contributes to the coupling action between piers. In their model, the slab acts as a flexural member, which – depending on the relative strengths of piers and spandrels – might form flexural hinges at the ends of the spandrel.

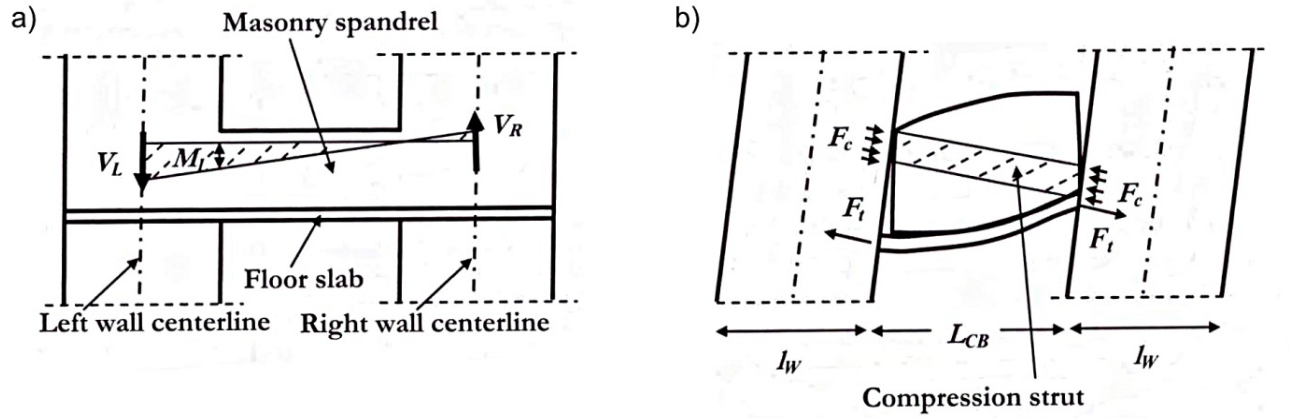

Figure 3. Internal forces of a composite spandrel (a). Assumed mechanical model of a composite spandrel including the compression diagonal in the masonry spandrel and the RC beam as tension member (b) [Priestley 2007].

Experimental evidence for composite spandrels

Five quasi-static tests on composite spandrels were carried out at the ETH Zurich [Beyer 2010]. All test units had the same outer dimensions as shown in Figure 4. The variables investigated concerned (i) the type of brick, (ii) the loading regime (monotonic / cyclic) and (iii) the longitudinal reinforcement content of the RC beams. For the following numerical investigations TU3 is used as a reference. TU3 was tested under cyclic loading and its crack pattern at failure is shown in Figure 5. A more in depth description of the experimental programme is presented in the companion paper [Dazio 2011].

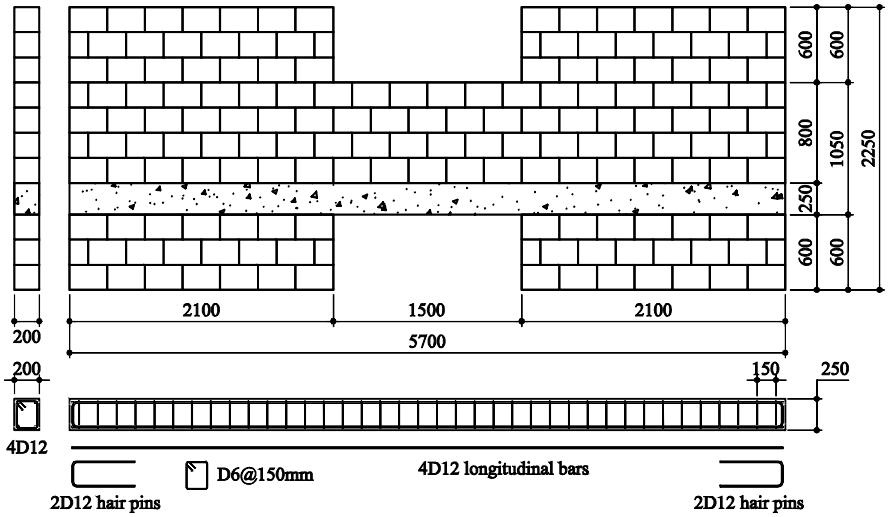

Figure 4. TU3: Geometry and reinforcing details of the test unit.

A simplified sketch of the observed mechanism is overlaid with the crack pattern of TU3 in Figure 5. The inclination of the compression strut in the masonry was not identical to the geometric diagonal of the spandrel but much steeper. The compression strut was supported

by the RC beam, which was subjected to positive bending at this position. Hence, the positive plastic hinge in the RC beam formed not at the end of the spandrel – as one would conclude if the masonry spandrel would be neglected – but within the spandrel. The negative plastic hinge in the RC beam, on the contrary, formed at the end of the spandrel. A further difference of the two plastic hinges concerned their length: While the negative plastic hinge was rather short the positive plastic hinge was typically spread over a longer part of the RC beam. In addition, a small gap opened between RC beam and masonry pier, which reduced the deformation demand on the RC beam. Final failure of TU3 was caused by the shear failure of the RC beam [Dazio 2011]. The mechanism observed during testing did therefore not correspond to the mechanisms shown in Figure 3, which form the basis for Eqs. 1 and 2.

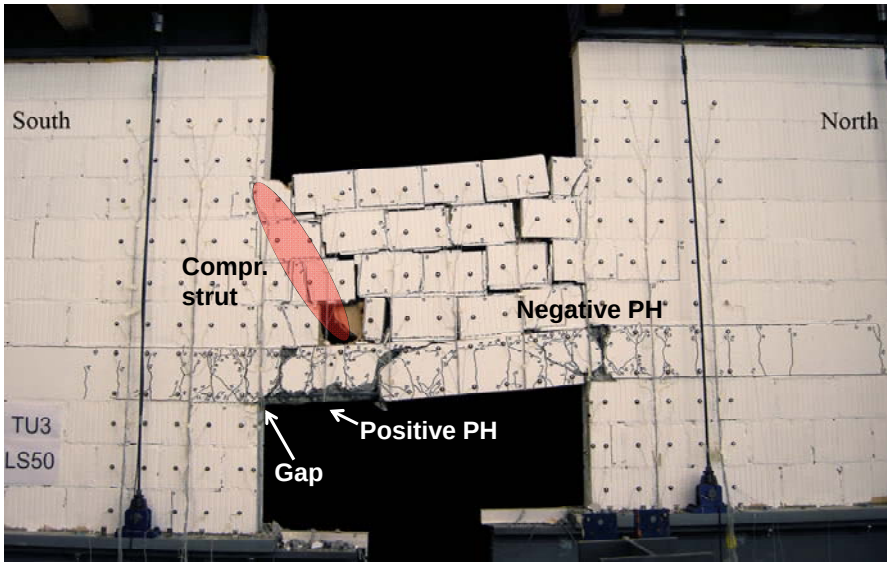

Figure 5. TU3: Crack pattern at failure and sketch of mechanism that formed.

Modeling of composite spandrels

The composite spandrels were analyzed using a simplified micro-modeling approach [Page 1978, Lourenço 1996]. In this model, each brick is modeled as a separate unit and the mortar joints are represented by contact elements. The RC beam was modeled using a concrete material model based on fracture mechanics. The longitudinal reinforcement bars were modeled as bar elements with perfect bond to the concrete while the shear reinforcement was implemented as smeared reinforcement. The numerical models were analyzed using the 2D version of the finite element programme Atena [Cervenka 2007].

The parameters for the constitutive laws for the masonry, concrete and reinforcing bars were derived from material tests that were carried out within the scope of the spandrel test programme. The constitutive law for the longitudinal reinforcing bars was an elasto-plastic relationship with an E-Modulus of E_s=200 GPa, a yield stress of f_y=540 MPa and a strain capacity of ε_{su}=7%. The concrete was modeled using the constitutive law “SBETA” with the

following material parameters: the E-Modulus E_c=31 GPa, the compressive strength f_c'=35.2 MPa, the strain at maximum stress ε_{cc}=0.17% and the tensile strength f_t=3.4 MPa. For the Poisson's ratio a value of ν=0.2 was assumed. The reinforcement properties were determined from monotonic tensile tests on bars with a clear length of 600 mm while the concrete material parameters were obtained from standard cylinder compression tests and double punch tests [Beyer 2010].

To characterize the masonry, tests on mortar and bricks as well as small masonry wallettes were carried out. The shear strength of the joints was obtained from standard tests on masonry triplets. The peak strength could be described by the following Mohr-Coulomb relationship:

$$\tau_{peak} = 0.71\sigma + 0.25 \quad \textbf{[3]}$$

This relationship was used to characterize the interface elements representing the mortar joints. The mortar joints were also assigned a tensile strength of f_t=0.35MPa. Compression tests on masonry wallettes were conducted for two different loading directions: For the X-direction-test the force was applied perpendicular to the bed joints while for the Y-direction-test the force was applied parallel to the bed joints. Photos of wallettes tested in X- and Y-direction are shown in Figure 6. The E-Modulus and compressive strength in X-direction were E_{mx}=5.3 GPa and f_{mx}=4.0 MPa, respectively. In the Y-direction the masonry was considerably softer (E_{my}=1.8 GPa) and weaker (f_{my}=1.3 MPa). For both directions a Poisson's ratio of 0.25 was assumed since the measured values were considered unreliable.

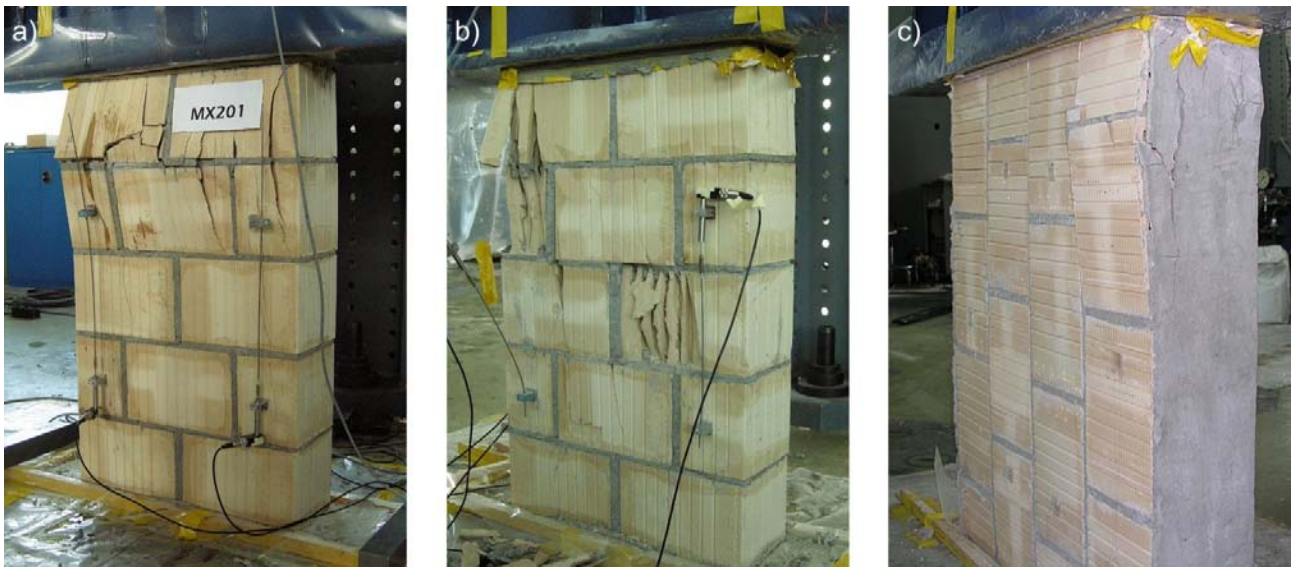

Figure 6. Compression tests on masonry wallettes in X-direction (perpendicular to bed joints, a+b) and in Y-direction (parallel to bed joints, c).

As a preparation for the analysis of the composite spandrels, the masonry wallettes of the compression tests were analyzed using the same simplified micro-modeling approach as for

the analysis of the composite spandrels. The material SBETA in Atena is a homogenous constitutive law, i.e. the material properties are the same for all directions of loading. For the compression tests, two different sets of material parameters were therefore defined, which represented the behavior in X- and Y-direction, respectively. For numerical reasons the joints cannot have an infinite stiffness. In the adopted modeling approach the joint stiffness has no physical meaning but was chosen to achieve a stable numerical convergence. To compensate for the joint flexibility the E-Modulus of the brick material had to be increased slightly (E_{mx}'=5.96 GPa, E_{my}'=1.90 GPa).

To simulate the test setup, steel beams were placed at the top and bottom of the wallettes (Figure 7). The analysis was carried out as a deformation controlled analysis, in this way also the post-peak behavior could be captured. Figure 7 shows the minimum principal strain at peak strength of the wallettes analyzed for compression in X- and Y-direction. Overlaid on the strain plot is the crack pattern. The cracks are plotted as black lines; the line thickness indicates the width of the cracks. For both directions of loading, the numerical simulations show a concentration of cracks at the centre of the wallettes. At the top and bottom the wallette was partially restrained by the steel beams and hence did not crack. For none of the two models the strain and crack profile was absolutely symmetric about the horizontal and vertical axes through the centre of the wallettes. While for the wallette tested in Y-direction this could be partly due to the asymmetric joint layout, the reason for the asymmetry of the result for the wallettes analyzed in X-direction must lie in numerical inaccuracies.

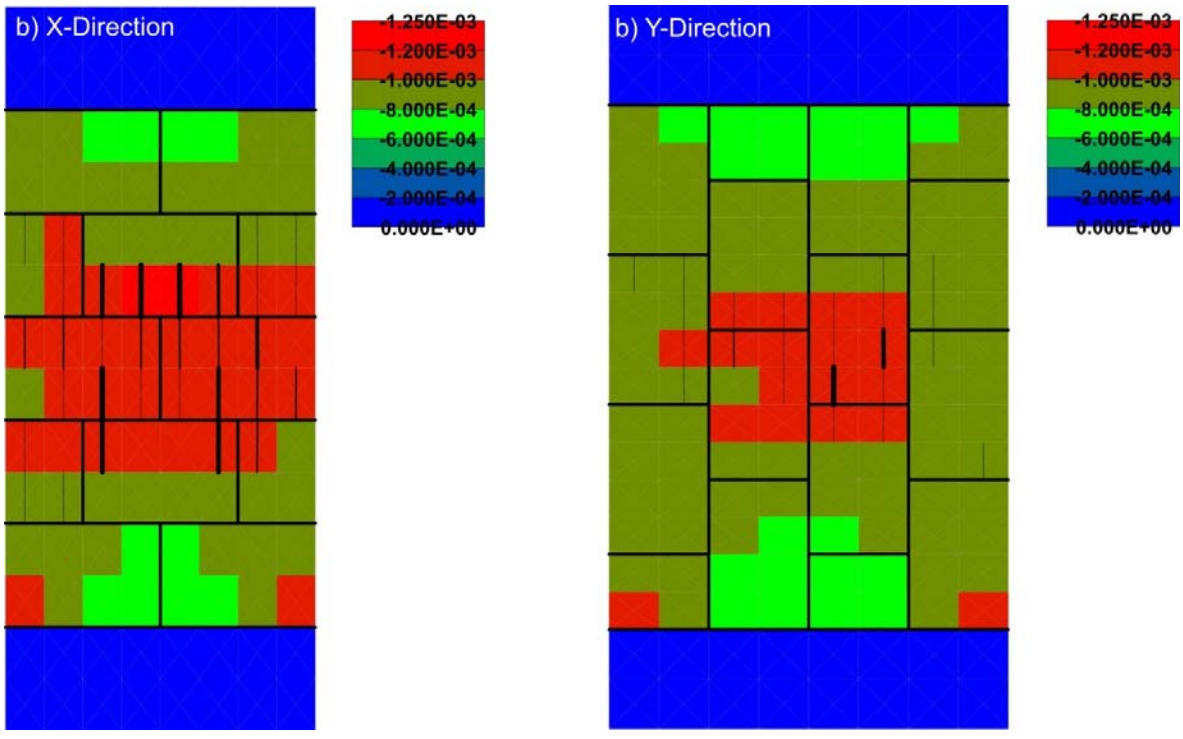

Figure 7. Minimum principal strain and crack pattern of numerical models for masonry compression tests at peak strength: X-direction (a) and Y-direction (b).

In the physical tests, the damage to the masonry wallettes was often concentrated in the upper half of the wallette (Figure 6a and c). Failure initiated typically with the formation of vertical cracks in the bricks and mortar joints. For loading in the Y-direction, horizontal and diagonal cracks followed. For both directions of loading the wallettes failed due to crushing of the outer brick shell. While in the physical wallettes the crack pattern was also controlled by the layout of the internal webs, the numerical models included homogenous full bricks. It was therefore not possible to draw from the numerical models detailed conclusions concerning the brick failure mode.

Figure 8 shows the comparison of the stress-strain curves obtained from the physical tests and the numerical analyses of the compression tests on the masonry wallettes. In the physical tests, the strain was obtained from four linear variable differential transformers (LVDT) readings with a base length of 600 mm. To achieve a good comparability between numerical and experimental results, the strain for the numerical model is computed from the vertical displacements of nodes that correspond approximately to the mounting points of the LVDT instruments. For both physical and numerical tests, the stress is computed as the applied axial force divided by the area of the nominal section. Figure 8 shows that the applied modeling approach simulates well the behavior up to the peak strength. The physical tests were carried out in a load controlled manner. Hence, the post-peak properties could not be obtained from experimental results and relatively arbitrary assumptions led to the shape of the post-peak behavior of the stress-strain curves for the numerical models.

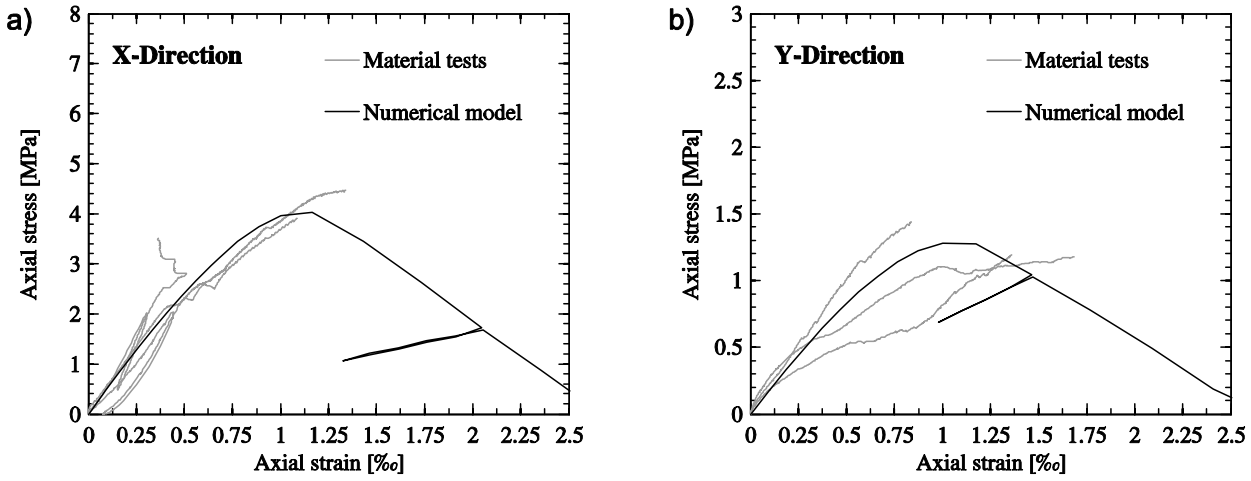

Figure 8. Comparison of stress-strain curves from masonry compression tests and numerical models: Compression test in the X-direction (a) and in the Y-direction (b).

Numerical analysis of composite spandrels and comparison to experimental results

The numerical model represents TU3, which was tested within the spandrel test programme under quasi-static cyclic loading. Note that comparison of cyclic and monotonic tests on composite spandrels showed that the loading type had little influence on the force envelope

[Beyer 2010]. The boundary conditions of the numerical model simulated the test setup for the spandrel test, where the pier deformation was imposed by the rotation of the lever beams, which supported the piers [Dazio 2011]. Two different models were analyzed: In the first model the bricks were modeled as elastic while in the second model the bricks were assigned the properties from the compression test in X-direction. In both models the bricks of the piers below the RC beam were assigned elastic properties. If also the lower bricks were modeled as inelastic, the brick at the edge of the pier below the negative plastic hinge was subjected to large compression strains leading to premature crushing. In the experiment such crushing of the brick had not been observed but the damage was typically limited to crushing of the mortar and some limited spalling of the brick. As a consequence, when modeling also the lower bricks as inelastic, the resulting deformation demand on the RC beam was too low.

Figure 9 shows in terms of the force-deformation curve the comparison of the numerical simulations to the experimental results. The curve resulting from the numerical model with elastic bricks envelopes the experimental results rather well up to the point where the capacity of the physical test unit dropped. It was outlined before that this drop in force seemed to be mainly associated with the crushing of the compression diagonal, which could not be captured by the model with elastic bricks. The sudden drops in strength for rotations between δ=0.3% and 0.5%, which were obtained for this numerical model, are associated with the opening of joints between bricks. The curve resulting from the model with inelastic bricks displayed a first significant loss in strength at about δ=0.55%. This rotation is considerably smaller than the rotation for which the physical test unit exhibited a drop in strength (~1.5%). However, the force level, which was attained after the drop in strength, is similar for the numerical and physical simulation. At a rotation of about δ=1.15% the numerical model with inelastic bricks did no longer converge.

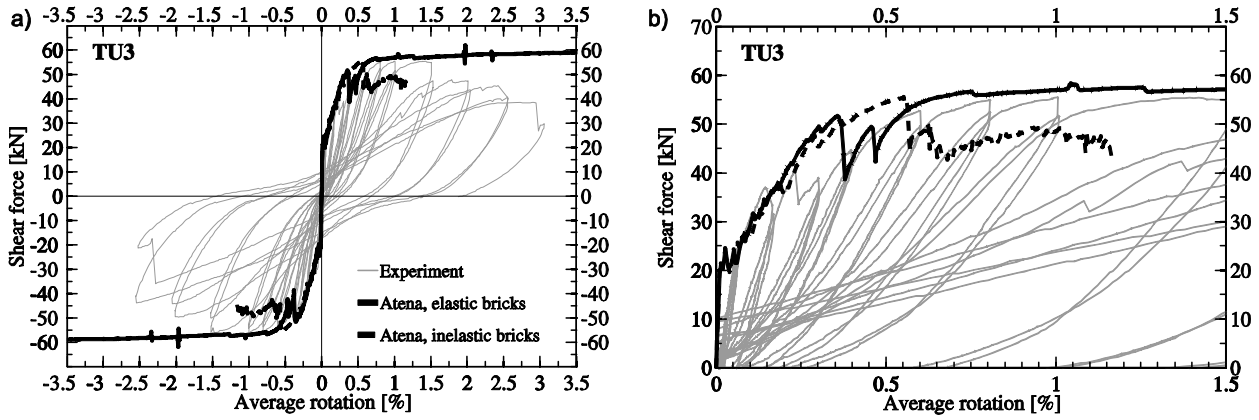

Figure 9. Comparison of force-deformation curves obtained for TU3 from experiments and numerical simulations.

Figures 10-12 show the principal strains, crack patterns and deformed shapes of the two numerical models when reaching the yield force. Before the onset of crushing of the compression diagonal in the masonry spandrel, the results of the models with elastic and inelastic bricks are almost identical (Figure 10 and 11). For the numerical model with inelastic

bricks the plot is provided for the state before and after the drop in strength (Figure 11 and 12, respectively). The strong damage concentration at two locations within the compression diagonal is clearly visible in Figure 12. Comparison with the observed crack pattern of masonry spandrel and RC beam (Figure 5) indicates that the numerical models is capable of reproducing the crack pattern of the masonry spandrel and the RC beam.

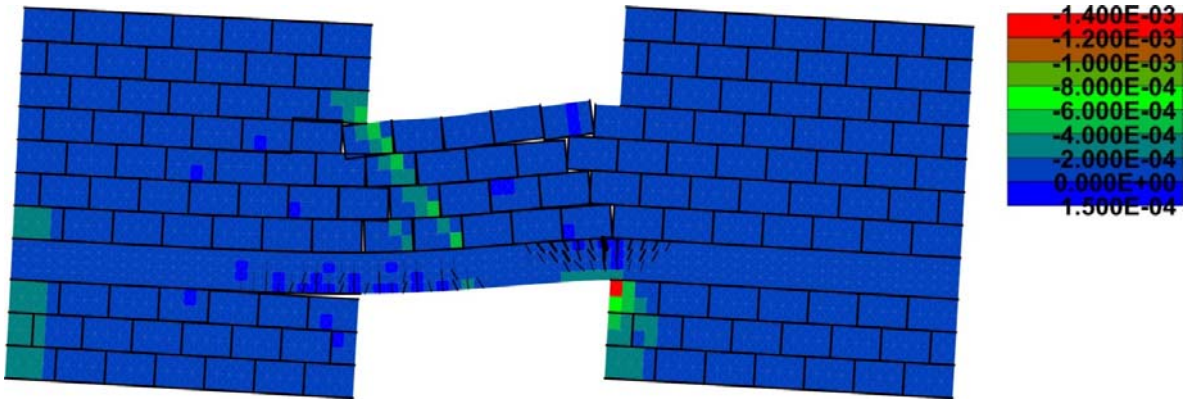

Figure 10. Numerical model with elastic bricks: Minimum principal strains, crack pattern and deformed shape (magnifying factor = 10) for a rotation of 0.6%.

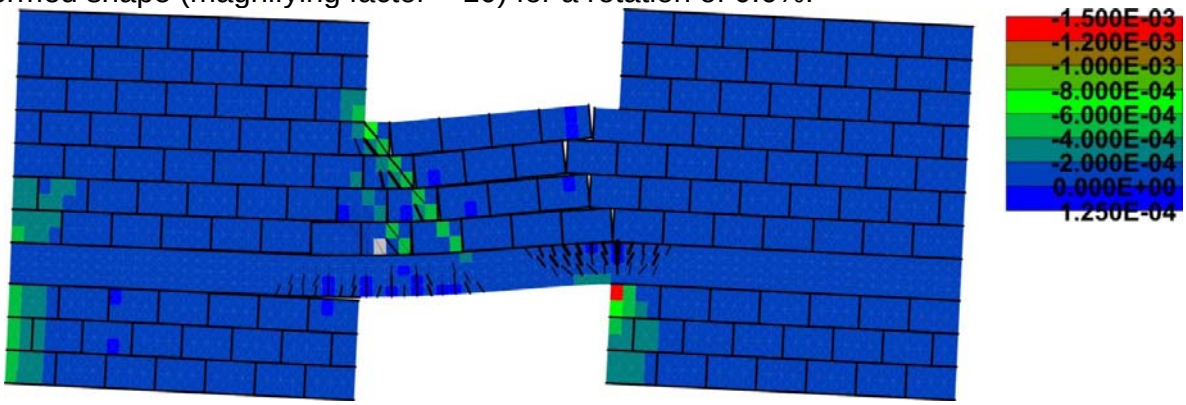

Figure 11. Numerical model with inelastic bricks: Minimum principal strains, crack pattern and deformed shape (magnifying factor = 10) for a rotation of 0.5%.

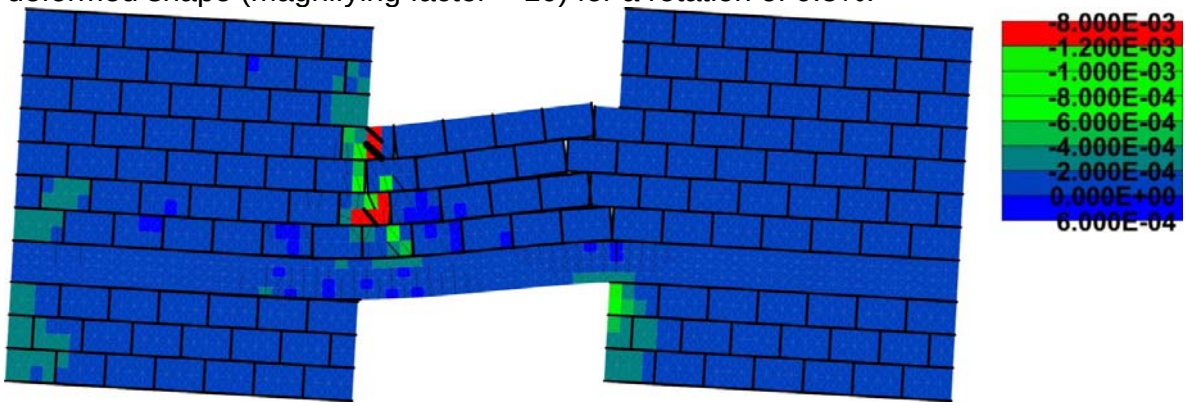

Figure 12. Numerical model with inelastic bricks: Minimum principal strains, crack pattern and deformed shape (magnifying factor = 10) for a rotation of 0.6%.

Analysis of different wall configurations of URM buildings

To investigate the behavior of composite spandrels in URM walls, a pushover analysis was carried out on the three story wall configuration shown in Figure 1b. The structure was modeled using the simplified micro-modeling approach with elastic bricks. Any failure mode involving crushing of the bricks can therefore not be captured by the model. Figure 13a shows the deformed shape of the URM wall at an average story drift of δ=0.4%. The average story drift was calculated as the horizontal displacement of the top floor slab divided by the height of the wall. The cracks in the RC beams indicate the locations where plastic hinges are forming in the beams. A comparison to the analysis results for the spandrel test unit (Figure 10) clearly indicates that the spandrel mechanisms obtained in the analysis of the isolated spandrel and the entire URM wall are rather similar. In both cases the positive plastic hinge is shifted inside the free length of the span and supports the compression strut in the masonry spandrel while the negative plastic hinge forms at the end of the spandrel.

Figure 13b shows the base shear-drift curve for the analyzed URM wall with composite spandrels in comparison to the same curve if the contribution of the composite spandrels was neglected. It shows that the spandrel action has a significant influence on both stiffness and strength of the URM wall and should therefore be considered in design and assessment of URM buildings.

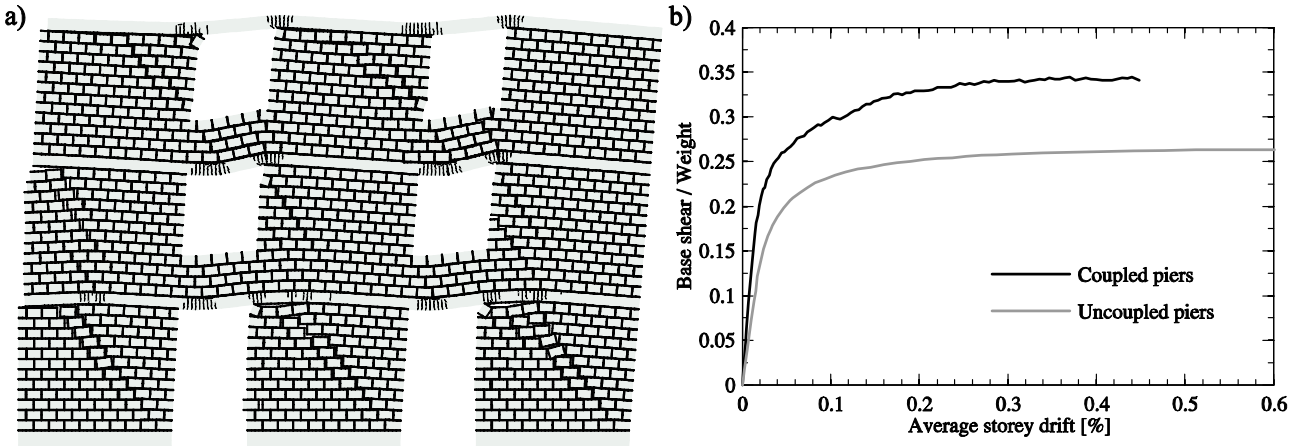

Figure 13. Deformed shape of the URM wall at an average story drift of δ=0.4% (a, displacements are magnified by a factor of 20) and pushover curve of the URM wall in comparison to the pushover curve of uncoupled piers (b).

Summary and conclusions

Composite spandrels are a common structural element in modern URM construction. Present recommendations for computing their strength are based on mechanical models that do not correspond to the mechanism observed during recent full-scale tests on composite spandrels. To understand better the behavior of the composite spandrels and to analyze

spandrel configurations that have not been tested, it is important to develop a numerical model that can capture the most important aspects of the composite spandrel when subjected to the deformation demand imposed by the rotation of the piers. The model should be able to capture the cracking of the RC beam and the formation of plastic hinges in the RC beam, the opening of joints as well as the formation of a compression strut in the masonry spandrel. The numerical model presented in this paper is a first step in this direction. It was shown that the behavior up to the maximum force can be captured rather well by models both with elastic or inelastic bricks. However, neither the deformation at which the spandrel started to loose strength, which in the experiments was associated with crushing of the compression diagonal, nor the limited deformation capacity of the RC beam could be captured by the current numerical models. Further work will therefore require an improvement of the model. It will also be attempted to link experimental and numerical limit states via strains. In the experiments optical measurements recorded the displacements of 180 LEDs on the spandrel from which average strains can be computed. From these measurements strain limits associated with certain limit states of the spandrel behavior will be determined.

References

Beyer 2010: Beyer, K., A. Abo-El-Ezz, A. Dazio, "Quasi-static cyclic tests on different types of masonry spandrels," Technical report, Institute of Structural Engineering, ETH Zurich, Switzerland, 2010.

Cervenka 2007: Cervenka, V., "Atena – Computer Program for Nonlinear Finite Element Analysis of Reinforced Concrete Structrues," Theory and User Manual, Prague, Czech Republic, 2007

Dazio 2011: Dazio, A., K. Beyer, "Experimental investigation of the longitudinal reinforcement content of ring beams on the cyclic behaviour of masonry spandrels," Proceedings of the 11th North American Masonry Conference, Minneapolis, 2011.

Lourenço 1996: Lourenço, P.B., "Computational strategies for masonry structures," PhD thesis, Technical University Delft, The Netherlands, 1996.

OPCM 2003: O.P.C.M. 3274, 20/03/2003. First elements concerning general criteria for the seismic classification of the national territory and technical norms for structures in seismic zone" (in Italian), Design Code OPCM 3274, 2003.

OPCM 2005: O.P.C.M. 3431/05, 09/05/2005. Further modifications and integrations on OPCM 3274/03" (in Italian), Design Code OPCAM 3431/05, 2005.

Page 1978: Page, A.W., "Finite element model for masonry," Journal of Structural Engineering 104(ST8), 1978, pp. 1267-1285.

Priestley 2007: Priestley, M.J.N., G.M. Calvi, M. Kowalsky, Displacement-based seismic design of structures, IUSS Press, Pavia, Italy, 2007.